Research Article Vol. 59, No. 19 / 1 July 2020 / Applied Optics 5715

applied optics

Geometry effects on luminescence solar concentrator efficiency: analytical treatment

Ilya Sychugov

KTH-Royal Institute of Technology, Department of Applied Physics, 16440 Kista-Stockholm, Sweden (e-mail: ilyas@kth.se)

Received 25 March 2020; revised 26 May 2020; accepted 26 May 2020; posted 26 May 2020 (Doc. ID 393521); published 25 June 2020

Luminescence solar concentrators act as semitransparent photovoltaic cells of interest for modern urban environments. Here, their efficiencies were analytically derived for different regular unit shapes as simple, integral-free expressions. This allowed analysis of the shape and size effect on the device performance. All regular shapes appear to have a similar efficiency as revealed by optical path distribution formulas, despite differences in the perimeter length. Rectangles of the same area feature higher efficiency due to reduced average optical path. It comes with the cost of a longer perimeter, and the relation between these two is provided. An explicit formula for the critical size of an LSC unit, above which its inner part becomes inactive, has been obtained. For square geometry with matrix absorption coefficient α this critical size is $\sim 2.7/\alpha$, corresponding to 70–90 cm for common polymer materials. Obtained results can be used for treatment of individual units as well as for analysis of tiling for large areas.

https://doi.org/10.1364/AO.393521

1. INTRODUCTION

Solar light spatial concentration through fluorophore re-emission in a planar waveguide was introduced long ago to reduce costs and improve the performance of solar cells [1]. It was mainly based on organic dyes, embedded in a plastic slab. However, dye molecules suffer from strong reabsorption losses, which seriously limited practical application of such luminescent solar concentrators (LSCs) [2,3]. Recent developments in quantum dots (QDs) make more favorable optical properties possible and thus bring the LSC concept closer to realization [4–7]. Covering large surfaces of, for example, facades of tall buildings with such semitransparent solar cells may be considered as one of the goals [8,9]. Here, the exact geometrical shape and size of the device unit may play an important role in the total efficiency.

Historically, the "concentration ratio" has been considered as a main figure of merit for an LSC. By now, the cost of solar cell modules ($/W) dropped by about three orders of magnitude compared with that of the early days of LSC research [10]. Therefore, reducing the area covered by solar cells and/or improving their performance by concentrating the incoming light flux may no longer be the primary motivation behind LSC development. In practice, attachment of solar cells only to one edge of an LSC was typically considered, i.e., an "LSCs for solar cell" approach [11,12]. Now, instead, possible modern applications include integration of such semitransparent modules in urban environments, where the full perimeter should be covered to increase the output power [13]. Here, the device efficiency of LSCs appears to be a more important parameter, even if it is associated with a nonoptimal solar cell performance or arrangement: a "solar cells for LSC" approach. From this application-driven perspective, the incorporation of all loss mechanisms in the device efficiency description is a necessary condition for adequate LSC analysis.

The analysis of optical losses in such planar waveguides is usually done by numerical integration [14] or by Monte Carlo ray tracing [13,15]. Indeed, simulations can follow evolution of nearly all aspects of the propagating light. In addition to its intensity, the spectrum, polarization, angle distribution, etc. can be tracked all the way to final distributions at the edges. In some cases, e.g., when only the total device efficiency needs to be estimated, such a complete and computationally demanding description may be redundant. We have previously shown that an analytical solution to the device efficiency can be obtained using only geometrical optics by probabilistic approach [16]. It was derived for a rectangular-shaped LSC as a function of the fluorophore and matrix parameters as well as device geometry.

Based on this analytical methodology, here we turned to the question of optimal size and shape for an LSC unit in a large assembly. Intuitively, one can associate two opposite effects with geometry of a single device. On the one hand, for a large area unit cell, the total perimeter length, hence the overall number of needed photodetectors, will be lower. On the other hand, large devices will suffer from more optical losses per unit and, hence, reduced efficiency. Indeed, the LSC operation is based on the waveguiding effect, therefore light scattering, re-absorption, and absorption in the matrix will become stronger. Here, we quantitatively assessed the interplay between these two effects

on examples of devices with common regular shapes and rectangle geometry. Based on the description, including all the losses, we show that, among regular shapes, a hexagon has the most favorable geometry. While the square is not far away in performance, a substantial enhancement can be achieved by enclosing the same area with rectangles. It comes with the cost of a longer perimeter, requiring more photodetectors, and the exact relation between these two parameters is provided. We have also derived a single, integral-free formula for the device efficiency in the case of a square-shaped LSC. More importantly, a simple criterion for the largest device size is introduced, which allows us to quickly evaluate limitations of a particular matrix material for LSC units.

2. SHAPE EFFECT

A. Regular Shapes

We start analysis by considering LSCs of regular shapes, enclosing the same area. As shown in Table 1, the perimeter length grows when shifting from a circle (radius R) to a triangle (side length b). In Table 1, the perimeter length is given in the units of a side length a of the same area square, where s is a hexagon side length.

First, we analytically derived the optical path length r distribution $p(r)$ for photons emanating from an isotropic emitter randomly located inside an LSC. Photodetectors with an antireflection coating are considered at all the edge surfaces. Derivations were done for various shapes and based on the algorithm used for a rectangle, as detailed in [16]. In essence, contributions from emitters on the arc with a radius r to the elementary edge element are summed up with subsequent integration over the edge length (see example for a circle in Appendix A1). At this stage, 2D geometry is considered and photons experience no attenuation. Results of analytical derivations were verified by the normalization condition: integrated expressions over the whole range of optical paths should be equal to the enclosed area. Below, the normalized (total integral is unity) probability density functions are presented. Thus, for a circle in a 2D case, the result is

$$p_c(r) = \frac{\sqrt{4R^2 - r^2}}{\pi R^2}, \quad 0 < r < 2R. \tag{1}$$

For a hexagon, the initial part is linear:

$$p_h(r) = \frac{4s - 2(1 - \pi\sqrt{3}/9)r}{s^2\pi\sqrt{3}}, \quad 0 < r < s, \tag{2}$$

with more complex expressions for the remaining $s < r < 2s$ (presented in Appendix A2). For a square, the distribution is piece-wise:

$$p_s(r) = \begin{cases} \frac{4a-2r}{\pi a^2}, & 0 < r < a \\ \frac{2r^2 - 4a\sqrt{r^2-a^2}}{\pi a^2 r}, & a < r < a\sqrt{2}. \end{cases} \tag{3}$$

For a triangle, the distribution is linear almost all the way:

$$p_t(r) = \frac{4\sqrt{3}b - \left(2\sqrt{3} + 4\pi/3\right)r}{\pi b^2}, \quad 0 < r < b\sqrt{3}/2. \tag{4}$$

The exact expression for the remaining short range $b\sqrt{3}/2 < r < b$ is given in Appendix A2.

The derived distributions are shown in Fig. 1 (left) and their first moments (average optical paths) in Table 1. From Fig. 1 (left), it is seen how a longer perimeter (from circle to triangle) increases the fraction of shorter optical paths. It stems from a larger part of emitters located close to the light-collecting edge. At the same time, increasing the perimeter also makes longer paths possible for the photons travelling across the unit.

These two effects largely compensate each other, making the average optical path similar for all considered regular shapes, as summarized in Table 1. Thus, increasing the perimeter length by ~30%, when choosing a triangle instead of a circle does not bring meaningful increase in optical efficiency (the average optical path stays nearly the same). This is a first conclusion of this work, which may not be so obvious without the explicit expressions in Eqs. (1)–(4) and Fig. 1 (left). As an independent verification of Eqs. (2)–(4), we note that, in [17], average optical paths were calculated by numerical integration, yielding the same results for these regular shapes.

Thus, considering optical losses, the best regular shape for such a planar waveguide obviously would be a circle. Here, the shortest perimeter is accompanied by nearly the same average optical path. Tiling without gaps, however, is not possible, and flexible solar cells are required in this case to accommodate the circular edge. A more practical shape would be a hexagon, which can be tiled over large surfaces without gaps and does not require special photodetectors at the edges. A square does not differ substantially from a hexagon in this respect. On the other hand, the most inefficient way of enclosing an area in this case is a triangle. This geometry also suffers from nonuniform incoming

Table 1. Perimeter Lengths and Average Optical Paths of Photons in Different Shape LSC with the Same Area[a]

Shape	Characteristic Size	Perimeter Length	Average Optical Path Length
Circle	$R = \pi^{-1/2} \approx 0.56$	3.55	$8\pi^{-3/2}/3 \approx 0.479$
Hexagon	$s = \sqrt{2}/3^{3/4} \approx 0.62$	3.72	0.478
Square	$a = 1$	4	$(2 + 6\ln(1+\sqrt{2}) - 2\sqrt{2})/3\pi \approx 0.473$
Triangle	$b = 2/3^{1/4} \approx 1.52$	4.56	0.461
Rectangle 1	$w = \beta^{-1/2} \approx 0.79$	4.12	0.467
$\beta = 1.62$	$h = \beta^{1/2} \approx 1.27$		
Rectangle 2	$w = \beta^{-1/2} \approx 0.59$	4.56	0.444
$\beta = 2.85$	$h = \beta^{1/2} \approx 1.69$		

[a]Units Are the Side Length of the Same Area Square.

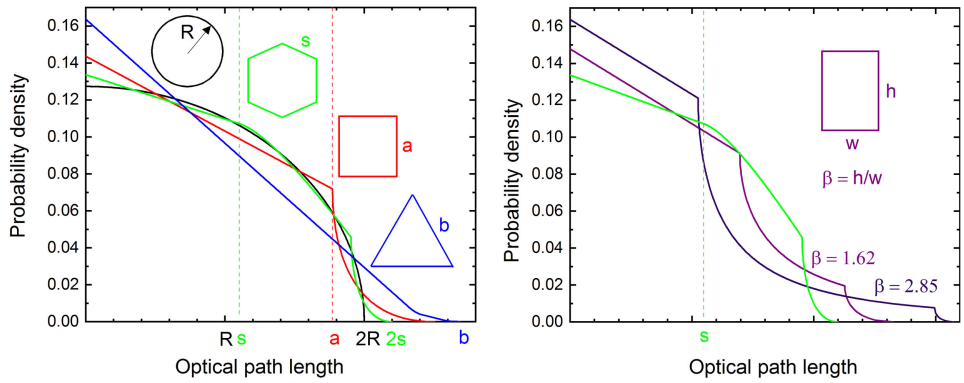

Fig. 1. Normalized probability density functions for an emitted photon to travel a given optical path length in luminescent solar concentrators of different shapes enclosing the same area. (left) Regular shapes are compared. (right) A hexagon is compared with the same area rectangles of two different aspect ratios.

light distribution along the edge, compared with other regular shapes [18].

B. Rectangle Shape

Expanding the selection of unit shapes to the irregular domain, one can immediately invoke a rectangle as an example, which is commonly used in modern large area facades. First, we need to introduce the rectangle aspect ratio β as an auxiliary parameter. An explicit expression for $p_r(r)$ is provided in Appendix A2. This normalized optical path probability distribution function for two values of β is shown in Fig. 1 (right). It is seen that a larger fraction of shorter optical paths exists for rectangles, which results in the lower average value.

Quantitatively, the average photon path $\langle r \rangle$ in a rectangular slab can be analytically calculated as a first moment of the given optical path distribution. The result is a decaying function of β (in units of the side length of the same area square):

$$\langle r \rangle_r = \frac{\beta^3 + 1 - (\beta^2+1)^{\frac{3}{2}} + 3\beta \ln\left(\sqrt{\beta^2+1}+\beta\right) + 3\beta^2 \ln\left(\frac{\sqrt{\beta^2+1}+1}{\beta}\right)}{3\pi\beta\sqrt{\beta}}. \tag{5}$$

Further, the perimeter length of such a rectangle is (in the same units)

$$P = \frac{2(\beta+1)}{\sqrt{\beta}}. \tag{6}$$

Numerical examples for two different rectangles are included in Table 1: the first corresponds to the well-known "golden ratio," and the second has the same perimeter length as the triangle. One can note that a rectangle with the same perimeter length as a triangle features lower optical losses. By further increasing perimeter (larger β), i.e., by deploying longer solar cells, the efficiency can be improved even more.

This effect is more clearly illustrated in Fig. 2, where the two functions from Eqs. (5) and (6) are shown. This graph shows how a longer perimeter helps to reduce an average optical path length for a rectangle, which is equivalent to reducing propagation losses in an LSC. The explicit effect on the total device efficiency, including all loss channels, will be shown later.

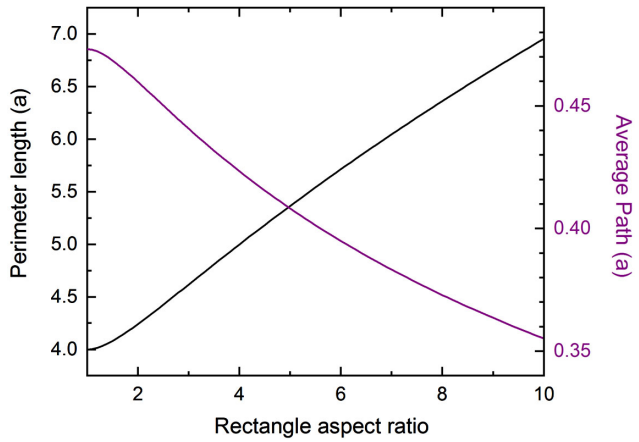

Fig. 2. (brown) Shortening of the average optical path for isotropic emitters in different aspect ratio rectangles, enclosing the same area [from Eq. (5)]. Units are the side length of the equivalent area square. (black) Related perimeter length increase is shown on the left axis [from Eq. (6)].

C. 3D Geometry

Before evaluating device efficiencies, we note that, for a 3D case, the optical paths will be extended on average by a factor of $k \approx 1.144$, for which an analytical expression is given in [16]. This is due to a narrow out-of-plane path distribution, which is limited by the escape cone. Here, emitted photons to the escape cone for the top and bottom surfaces are treated as losses. Total internal reflection is assumed for all other directions. A similar factor of 1.128 was used in [17] to account for an average optical path increase due to the out-of-plane emission. A small difference stems from the fact that, in [17], the numerical averaging was performed over angles not over optical paths. Thus, 3D distributions for all the shapes can be represented as $q(l) \approx p(l/k)$. For example, in a circle the normalized probability density function becomes

$$q_c(l) = \frac{\sqrt{4R^2 - (l/k)^2}}{\pi k R^2}, \quad 0 < l < 2Rk. \tag{7}$$

Explicit expression for the optical path distributions for other shapes in 3D are provided in the Appendix A3.

3. CRITICAL SIZE

A. Regular Shapes

Analytical expressions for $q(l)$ allow us to obtain explicitly the fraction of emitted light reaching the edge of the device, i.e., the waveguiding or optical efficiency [%]:

$$f(\alpha) = \int_0^{l_{\max}} q(l) \exp(-\alpha l)\, \mathrm{d}l, \tag{8}$$

where $l_{\max}$ is the longest optical path in the system. Physically, it corresponds to the optical efficiency when the only loss mechanism is the matrix absorption (with a loss parameter being the matrix absorption coefficient $\alpha = \alpha_m$ [cm^{-1}]). For a circle ($l_{\max} = 2Rk$), the integral yields

$$f_c(\alpha) = -\frac{M_1(2\alpha Rk)}{\alpha Rk}, \tag{9}$$

where $M_1(\xi)$ is a modified Struve function of the second kind: $M_1(\xi) = L_1(\xi) - I_1(\xi)$, where $I_1(\xi)$ is a modified Bessel function, and $L_1(\xi)$ is a modified Struve function (all functions are of the first order). Analytical expressions of $f(\alpha)$ for other shapes are provided in the Appendix A4. Equation (9) can be simplified for large arguments, using expansion of $M_1(\xi)$ (shown in the Appendix A5) and leaving only the first term (a constant $-2/\pi$):

$$f_c(\alpha) \approx \frac{2}{\alpha R\pi k}, \quad \alpha R \to \infty. \tag{10}$$

In Fig. 3, these two expressions are shown in a log-log scale as a function of the dimensionless parameter αR [as a solid line for Eq. (9) and as a dotted line for Eq. (10)].

A qualitative meaning of the function $f(\alpha)$ is the fraction of the total area, from which the emanated emission reaches the edge. In the lack of attenuation, the whole area contributes,

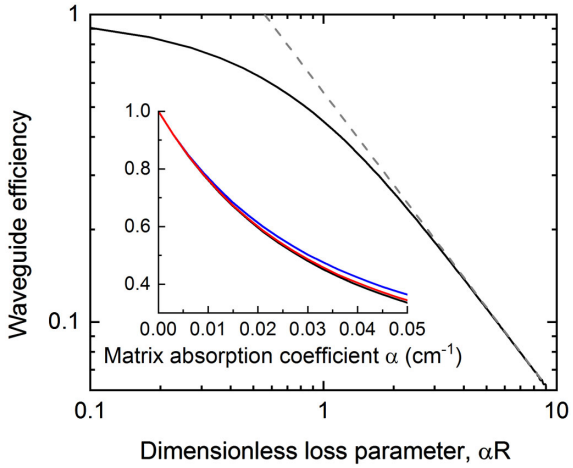

Fig. 3. Dependence of the waveguiding efficiency of the dimensionless parameter αR. A dotted line is an asymptotic from Eq. (10); the solid line is a full expression from Eq. (9). Inset shows waveguide efficiencies for a circle (black), a square (red), and a triangle (blue) for the same area units ($R = 30$ cm).

yielding optical efficiency unity. Here, we postulate that the transition from Eqs. (9) to (10) signifies a critical size of the device. Indeed, in the presence of absorption, only the emission close to the edge will be collected in large area devices. If the thickness of this active part is Δ ($\Delta \sim 1/\alpha$), its area is about $2\pi R\Delta$. Thus, the useful fraction of the total area πR^2 becomes proportional to $(\alpha R)^{-1}$. This is exactly the dependence Eq. (10) predicts. In this case, the emitted light from the central part is lost; thus, a device is no longer operating as a proper LSC. Therefore, in practice, it makes no sense to fabricate units larger than this critical size, which will render the inner part inactive.

Numerically, the value of the critical dimensionless parameter can be extracted at the point in Fig. 3 where these two curves start converging. While this point cannot be precisely defined, we can estimate its position from the principle of experimental significance. A deviation of a few percent from Eq. (10) can be measurable. Thus, one can stipulate that, when Eq. (9) differs from Eq. (10) by more than 3% to 5%, the contribution from the inner part should not be ignored. From Fig. 3, for $\alpha R = 1$ the relative difference in efficiency is ~10%, while for $\alpha R = 2$ it is only ~1%. Thus, for a circle, one can approximately set $\alpha \cdot R_{\mathrm{cr}} \leq 1.5$, where the difference is ~3%. Assuming the same optical path distribution (cf. Fig. 1), the criteria for a hexagon, enclosing the same area, is $\alpha \cdot s_{\mathrm{cr}} \leq 1.7$, while for a square,

$$\alpha \cdot a_{\mathrm{cr}} \leq 2.7. \tag{11}$$

This is a second important conclusion of the presented analysis: a way to quickly estimate maximum useful LSC unit size is proposed. As a numerical example, consider typical polymers, such as PMMA or OSTE with $\alpha \approx 0.03 - 0.04\ \mathrm{cm}^{-1}$ as a matrix material [13,19]. Then, according to Eq. (11), a square unit with a side length not more than ~70 − 90 cm should be used. In further analysis, we will limit considered device sizes by this criterion.

To illustrate negligible effect of the regular shape choice on optical losses, one can compare derived expressions $f(\alpha)$ for LSCs enclosing the same area. Those are shown for a circle (black), a square (red), and a triangle (blue) in Fig. 3, inset ($R = 30$ cm). The x axis is limited by the LSC critical parameter, as defined above. These functions essentially coincide for a small value of the loss parameter and deviate only by 1%–2% for larger α in case of a triangle. Thus, the regular shapes considered here indeed have similar waveguiding efficiencies, as was also concluded from the average optical path comparison. This is despite a large difference in the perimeter length (cf. Table 1). Therefore, we propose to use Eq. (9) as an approximation for all the shapes, except for the triangle. With this assumption, simple expressions for the total LSC device efficiency can be derived for these geometries.

B. Rectangle Shape

The size limit for a rectangle can also be evaluated from the obtained criterion. Here, we do not consider rectangles of the same area as regular shapes but define the maximum useful aspect ratio for a given width. Note that it cannot be defined as clearly as for the case of a square, where the inner part becomes simply inactive. However, we can set the average optical path, corresponding to the critical size a_{cr}, as a critical optical path.

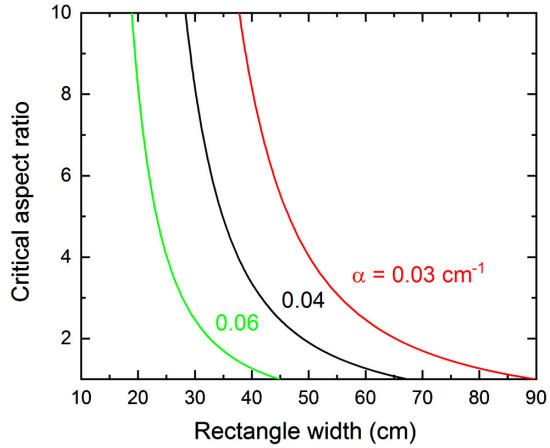

Fig. 4. Critical aspect ratio of a rectangle LSC as a function of width for different absorption coefficients.

Then, the critical rectangle width [cm], corresponding to this average path, can be expressed as a function of the absorption coefficient $\alpha[\mathrm{cm}^{-1}]$ and the aspect ratio β from Eqs. (5) and (11) and Table 1:

$$w_{\mathrm{cr}} \approx \frac{12\beta}{\alpha\left(\beta^3+1-\left(\beta^2+1\right)^{\frac{3}{2}}+3\beta\ln\left(\sqrt{\beta^2+1}+\beta\right)+3\beta^2\ln\left(\sqrt{\beta^2+1}+1\right)-3\beta^2\ln\left(\beta\right)\right)}. \tag{12}$$

Examples for some relevant matrix absorption coefficients are presented in Fig. 4. It is shown instead as inverse function $\beta_{\mathrm{cr}}(w)$, which indicates what the maximum aspect ratio can be tolerated for a given rectangle width.

4. DEVICE OPTICAL EFFICIENCY

A. Analytical Expression

For more realistic description of the device performance, other loss mechanisms need to be considered. Those included losses from scattering and reabsorption by the fluorophores. In general, the LSC optical efficiency γ [%] in the case of all possible losses can be evaluated using the waveguide efficiency function $f(\alpha)$ using geometrical sum series as [16]

$$\gamma = \frac{(1-T)\cdot\delta\cdot\mathrm{QY}\cdot\eta\cdot f(\alpha_{\mathrm{sc}}+\alpha_{\mathrm{re}}+\alpha_m)}{1-\frac{\delta\cdot\alpha_{\mathrm{sc}}+\delta\cdot\mathrm{QY}\cdot\alpha_{\mathrm{re}}}{\alpha_{\mathrm{sc}}+\alpha_{\mathrm{re}}+\alpha_m}\left(1-f(\alpha_{\mathrm{sc}}+\alpha_{\mathrm{re}}+\alpha_m)\right)}. \tag{13}$$

Here, T is a transmitted fraction of the incoming sunlight ($1-T$ is the absorbed fraction). Parameter $\eta=\epsilon_{\mathrm{PL}}/\epsilon_{\mathrm{sun}}$ is the energy conversion coefficient of the luminescence, defined as the ratio of luminescence and solar peak position energies. QY is the quantum yield, and δ is a fraction of the emission to the waveguiding mode ($\delta=75\%$ for $n=1.5$ matrix material). The linear reabsorption coefficient is $\alpha_{\mathrm{re}}[\mathrm{cm}^{-1}]$, the linear scattering coefficient is $\alpha_{\mathrm{sc}}[\mathrm{cm}^{-1}]$, and the linear matrix absorption coefficient is $\alpha_m[\mathrm{cm}^{-1}]$. These should be taken for the wavelength of the fluorophore luminescence (corresponding to ϵ_{PL}).

For a square shape, using Eq. (9), the resulting expression can be represented as a relatively simple formula (with $\alpha=\alpha_{\mathrm{sc}}+\alpha_{\mathrm{re}}+\alpha_m$ as a loss parameter and $R=a/\sqrt{\pi}$):

$$\gamma_s = \frac{(1-T)\cdot\delta\cdot\mathrm{QY}\cdot\eta\cdot M_1(2\alpha a k/\sqrt{\pi})\cdot\alpha\sqrt{\pi}}{\delta(\alpha_{\mathrm{sc}}+\mathrm{QY}\cdot\alpha_{\mathrm{re}})\left(ak\alpha+M_1(2\alpha a k/\sqrt{\pi})\cdot\sqrt{\pi}\right)-ak\alpha^2}. \tag{14}$$

As justified above, it can also be used for hexagons with $a=1.62\cdot s$ and for circles with $a=R\cdot\sqrt{\pi}$. Equation (14) yields device efficiency for a square-shaped LSC without any integral representations, as contained in a more general formula for the rectangle [16]. We mark this as another important result of the presented analysis: a single integral-free formula for the efficiency a square-shaped LSC was derived. Multiplying Eq. (14) by Φa^2 (solar flux $\Phi=0.1\ \mathrm{W/cm}^2$) gives optical efficiency in [W]. Reflectance of the solar radiation is not explicitly included because back-travelling light will also contribute to the incoming power. Therefore, the standard AM1.5 irradiance is used for simplicity.

Unlike Eq. (9), where the only loss mechanism is matrix absorption, the total output here is not a function of a dimensionless parameter αa. The loss parameter α and the waveguide geometry act as two independent parameters. So, instead of a general criterion for establishing the critical size, the device performance for each particular material system should be evaluated. The criteria of Eq. (11) and Fig. 4 then represent an upper limit.

B. Comparison with Experiment

To illustrate this result and to compare it with experiments, we turn to Si QDs as fluorophores. They are often considered as candidates for this application due to a large Stokes shift and a good quantum yield [13,19,20]. In Fig. 5, theoretical lines of the LSC efficiency in [%] (solid) and in [W] (dashed) are presented for a square geometry [Eq. (14)]. The fluorophore parameters are taken from the experiment [21]: QY = 55%, transparency for visible light $T_1=0.79$ (3 mm thick film), and $T_2=0.62$ (6 mm thick film), reabsorption coefficient $\alpha_{\mathrm{re}}=0.007\ \mathrm{cm}^{-1}$, scattering coefficients $\alpha_{\mathrm{sc\_1}}=0.04\ \mathrm{cm}^{-1}$ (3 mm thick film), $\alpha_{\mathrm{sc\_2}}=0.06\ \mathrm{cm}^{-1}$ (6 mm thick film), matrix absorption coefficient $\alpha_m=0.04\ \mathrm{cm}^{-1}$, and $\eta=0.6$.

Experimental results for the optical power efficiency were obtained by measuring the short-circuit current of the attached photodetectors [21]. In the experiment, antireflection photodetectors were realized by using solar cells with a porous polymer film as a gradient-refractive-index coating. Those were attached with index-matching optical glue to avoid an air gap. Measured values of ~3.7% for the 9 cm × 9 cm × 0.3 cm piece and ~7.9% for the 9 cm × 9 cm × 0.6 cm device are indeed within the experimental error from the predictions of Eq. (14).

A practically important electrical power output is characterized by the power conversion efficiency (PCE, [%]). Using Eq. (14) for the optical power efficiency, we can evaluate this quantity. First, one should invoke external quantum efficiency

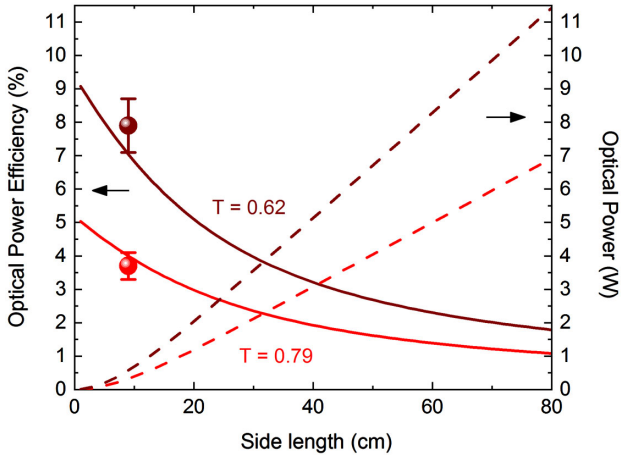

Fig. 5. Device efficiency and corresponding optical power output for Si QD-based devices of square geometry with different transmission [from Eq. (14)]. Experimental points are from measurements of a 9×9 cm^2 device with 3 mm (red) and 6 mm (brown) thickness of the active layer [21].

(EQE) of the solar cells, which is a photon-to-electron conversion efficiency at the device readout. Then, a lower bandgap of the solar cell material (ϵ_g) needs to be considered (energy conversion coefficient $\eta_1 = \epsilon_g/\epsilon_{\mathrm{PL}}$). Finally, a working voltage point of a solar cell is lower than the bandgap and is characterized by the fill factor (FF) coefficient. Combining these loss factors together for a square geometry, one can write

$$\mathrm{PCE} = \mathrm{EQE} \cdot \eta_1 \cdot \mathrm{FF} \cdot \gamma_s. \tag{15}$$

For Si solar cells, such as the ones used in the experiment [21], the EQE at the PL wavelength (850 nm) is $\sim 0.8 - 0.9$, a typical fill factor is ~ 0.7, and the energy conversion coefficient is $\eta_1 \approx 0.7$. Thus, in this case, one can evaluate theoretically $\mathrm{PCE} \approx 0.4 \cdot \gamma_s$, which becomes 1.6% and 2.8% for the two cases in Fig. 5 (9 cm × 9 cm). Experimentally measured values are 1.47% and 2.74%, respectively [21], which is again close to the theoretical predictions. For the reader's convenience, we have added Origin files with formulas for efficiency calculations (both for square and for rectangle) as Dataset 1, Ref. [22] and Dataset 2, Ref. [23].

5. CONCLUSION

We have derived analytical formulas for the optical path distribution for an isotropic emitter randomly placed in a planar waveguide of different shapes. Resulting expressions were used for the analysis of LSC performance as interplay between the perimeter length and the propagation losses. Among regular shapes, hexagons and squares have the best perimeter/loss combination and can be considered as unit shapes for large area tiling. On other hand, at the expense of somewhat longer perimeter length, the same area rectangle yields better collection efficiency due to suppression of the longer optical path lengths. Simple criteria for the critical unit size were obtained. The effect of the size increase on the total device power output was quantitatively demonstrated for a given material system with a good match to the experiment.

APPENDIX A

1. DERIVATIONS OF THE PROBABILITY DENSITY FUNCTION OF OPTICAL PATHS FOR A CIRCLE

Consider contributions to the length element dy from isotropic emitters located on the arc at a radius r from dy. If $\theta_{1,2}$ are the limiting angles of the arc the incoming signal to dy,

$$F = \frac{dy}{2\pi}\int_{\theta_1}^{\theta_2} \sin(\theta)\mathrm{d}\theta = \frac{dy}{2\pi}(\cos(\theta_1) - \cos(\theta_2)).$$

Integrating contributions over the whole perimeter edge gives probability distribution for photons to travel path r:

$$p(r) = \frac{1}{2\pi}\int_0^{2\pi R} (\cos(\theta_1) - \cos(\theta_2))\mathrm{d}y$$

$$= R(\cos(\theta_1) - \cos(\theta_2)) = \sqrt{4R^2 - r^2},$$

where $\theta_1 = 90 - \alpha$; $\theta_2 = 90 + \alpha$, for $\cos(\alpha) = \frac{r/2}{R}$. A properly normalized probability density function can be then obtained by dividing by the area under the curve:

$$p(r) = \frac{\sqrt{4R^2 - r^2}}{\pi R^2}.$$

2. OPTICAL PATH LENGTH DISTRIBUTION IN 2D

For a hexagon with a side length s

$$p_h(r) = \begin{cases} \frac{4s - 2(1-\pi\sqrt{3}/9)r}{s^2\pi\sqrt{3}}, & 0 < r < s \\ \frac{2s\sqrt{4r^2-3s^2}}{\sqrt{3}\pi r s^2} - \frac{2r}{3\pi s^2}\mathrm{asin}\left(\frac{s\sqrt{3}(2r^2-3s^2)\sqrt{4r^2-3s^2}}{2r^4}\right), & s < r < s\sqrt{3} \\ \frac{2r^2-8s\sqrt{r^2-3s^2}}{\sqrt{3}\pi r s^2} + \frac{2r}{3\pi s^2}\mathrm{asin}\left(\frac{\sqrt{3}(r^2-6s^2+2s\sqrt{r^2-3s^2})}{2r^2}\right), & s\sqrt{3} < r < 2s. \end{cases}$$

For a rectangle with aspect ratio β and width w ($\beta > 1$),

$$p_r(r) = \begin{cases} \frac{2w + 2\beta w - 2r}{\pi\beta c^2}, & 0 < r < w \\ \frac{2r - 2\sqrt{r^2-w^2}}{\pi w r}, & w < r < \beta w \\ \frac{2r^2 - 2\beta w\sqrt{r^2-w^2} - 2w\sqrt{r^2-\beta^2 w^2}}{\pi\beta w^2 r}, & \beta w < r < w\sqrt{\beta^2+1}. \end{cases}$$

For a triangle with side length b,

$$p_t(r) = \begin{cases} \frac{4\sqrt{3}b - (2\sqrt{3}+4\pi/3)r}{\pi b^2}, & 0 < r < b\sqrt{3}/2 \\ u(r), & b\sqrt{3}/2 < r < b. \end{cases}$$

$$u(r)=\frac{4\sqrt{3}}{\pi b^2}\left(b-\left(\frac{1}{2}-\frac{\pi\sqrt{3}}{18}\right)r-\frac{b\sqrt{4r^2-3b^2}}{2r}\right.$$
$$+\frac{r\sqrt{3}}{6}\left(\operatorname{asin}\left(\frac{\sqrt{3}(\sqrt{4r^2-3b^2}-b)}{4r}\right)\right.$$
$$\left.\left.+\operatorname{asin}\left(\frac{\sqrt{3}(\sqrt{4r^2-3b^2}+b)}{4r}\right)-2\operatorname{asin}\left(\frac{\sqrt{3}b}{2r}\right)\right)\right)$$

3. OPTICAL PATH LENGTH DISTRIBUTION IN 3D

For a 3D case in hexagon, the properly normalized distribution function can be considered the same as in a circle for the same enclosed area: $R=3^{3/4}s/\sqrt{2\pi}=c_0\cdot s,\ c_0\approx 0.91\ (k\approx 1.14)$

$$q_h(l)\approx\frac{\sqrt{4c_0{}^2s^2-(l/k)^2}}{\pi k c_0{}^2 s^2},\quad 0<l<2c_0 s k.$$

For a triangle, considering only the linear part of the optical path distribution:

$$q_t(l)=\frac{4\sqrt{3}b-\left(2\sqrt{3}+4\pi/3\right)(l/k)}{\pi k b^2},\quad 0<l<bk\sqrt{3}/2.$$

For a square,

$$q_s(l)=\begin{cases}\frac{4a-2(l/k)}{\pi k a^2}, & 0<l<ka\\ \frac{2l^2/k-4a\sqrt{l^2-(ka)^2}}{\pi a^2 lk}, & ka<l<ka\sqrt{2}.\end{cases}$$

4. WAVEGUIDING EFFICIENCY

For a square (x is a loss parameter)

$$f_s(x)=\frac{2\left(2axk-\left(ka\sqrt{2}x+1\right)\cdot e^{-ka\sqrt{2}x}+2e^{-kax}-1\right)}{x^2a^2\pi k^2}$$
$$-\frac{4}{a\pi k}\int_{ka}^{ka\sqrt{2}}\frac{\sqrt{l^2-(ka)^2}}{l}\exp(-xl)\,\mathrm{d}l.$$

For a triangle,

$$f_t(x)=\frac{e^{-\frac{kb\sqrt{3}x}{2}}\left(6\sqrt{3}-2\sqrt{3}bkx\,(6-\pi)+9bkx+4\pi\right)+12\sqrt{3}bkx-4\pi-6\sqrt{3}}{3x^2b^2\pi k^2}.$$

For a rectangle (height h, width w, diagonal d),

$$f_r(x)=2\left(\frac{(h+w)\,xk-(kdx+1)\,e^{-kdx}+e^{-khx}+e^{-kwx}-1}{x^2hw\pi k^2}\right.$$
$$\left.-\int_{kw}^{kd}\frac{\sqrt{l^2-(kw)^2}}{w\pi kl}e^{-xl}\mathrm{d}l-\int_{kh}^{kd}\frac{\sqrt{l^2-(kh)^2}}{h\pi kl}e^{-xl}\mathrm{d}l\right).$$

5. EXPANSION OF THE MODIFIED STRUVE FUNCTION OF THE SECOND KIND (FIRST ORDER) FOR $\xi\to\infty$ (see, e.g., https://dlmf.nist.gov/11.6)

$$M_1(\xi)\approx\frac{1}{\pi}\sum_{k=0}^{\infty}(-1)^{k+1}\frac{\Gamma\left(k+\frac{1}{2}\right)}{\Gamma\left(\frac{3}{2}-k\right)}\left(\frac{2}{\xi}\right)^{2k}=-\frac{2}{\pi}+\frac{2}{\pi\xi^2}-\cdots$$

Funding. Energimyndigheten (46360-1).

Disclosures. The authors declare no conflict of interests.

REFERENCES

1. J. S. Batchelder, A. H. Zewail, and T. Cole, "Luminescent solar concentrators 2. Experimental and theoretical analysis of their possible efficiencies," Appl. Opt. **20**, 3733–3754 (1981).
2. R. W. Olson, R. F. Loring, and M. D. Fayer, "Luminescent solar concentrators and the reabsorption problem," Appl. Opt. **20**, 2934–2940 (1981).
3. J. Sansregret, J. M. Drake, W. R. L. Thomas, and M. L. Lesiecki, "Light transport in planar luminescent solar concentrators—the role of DCM self-absorption," Appl. Opt. **22**, 573–577 (1983).
4. Z. Krumer, S. J. Pera, R. J. A. van Dijk-Moes, Y. Zhao, A. F. P. de Brouwer, E. Groeneveld, W. G. J. H. M. van Sark, R. E. I. Schropp, and C. de Mello Donegá, "Tackling self-absorption in luminescent solar concentrators with type-II colloidal quantum dots," Sol. Energy Mater. Sol. Cells **111**, 57–65 (2013).
5. A. Anand, M. L. Zaffalon, G. Gariano, A. Camellini, M. Gandini, R. Brescia, C. Capitani, F. Bruni, V. Pinchetti, M. Zavelani-Rossi, F. Meinardi, S. A. Crooker, and S. Brovelli, "Evidence for the band-edge exciton of CuInS2 nanocrystals enables record efficient large-area luminescent solar concentrators," Adv. Funct. Mater. **29**, 1906629 (2019).
6. F. Meinardi, A. Colombo, K. A. Velizhanin, R. Simonutti, M. Lorenzon, L. Beverina, R. Viswanatha, V. I. Klimov, and S. Brovelli, "Large-area luminescent solar concentrators based on 'Stokes-shift-engineered' nanocrystals in a mass-polymerized PMMA matrix," Nat. Photonics **8**, 392–399 (2014).
7. L. R. Bradshaw, K. E. Knowles, S. McDowall, and D. R. Gamelin, "Nanocrystals for luminescent solar concentrators," Nano Lett. **15**, 1315–1323 (2015).
8. M. Rafiee, S. Chandra, H. Ahmed, and S. J. McCormack, "An overview of various configurations of luminescent solar concentrators for photovoltaic applications," Opt. Mater. **91**, 212–227 (2019).
9. Y. You, X. Tong, W. Wang, J. Sun, P. Yu, H. Ji, X. Niu, and Z. M. Wang, "Eco-friendly colloidal quantum dot-based luminescent solar concentrators," Adv. Sci. **6**, 1801967 (2019).
10. X. T. Wang and A. Barnett, "The evolving value of photovoltaic module efficiency," Appl. Sci. **9**, 1227 (2019).
11. E. Loh and D. J. Scalapino, "Luminescent solar concentrators—effects of shape on efficiency," Appl. Opt. **25**, 1901–1907 (1986).
12. B. Rowan, S. McCormack, J. Doran, and B. Norton, "Quantum dot solar concentrators: an investigation of various geometries," Proc. SPIE **6649**, 66490A (2007).
13. F. Meinardi, S. Ehrenberg, L. Dhamo, F. Carulli, M. Mauri, F. Bruni, R. Simonutti, U. Kortshagen, and S. Brovelli, "Highly efficient luminescent solar concentrators based on earth-abundant indirect-bandgap silicon quantum dots," Nat. Photonics **11**, 177–185 (2017).
14. O. M. ten Kate, K. M. Hooning, and E. van der Kolk, "Quantifying self-absorption losses in luminescent solar concentrators," Appl. Opt. **53**, 5238–5245 (2014).
15. N. D. Bronstein, L. F. Li, L. Xu, Y. Yao, V. E. Ferry, A. P. Alivisatos, and R. G. Nuzzo, "Luminescent solar concentration with semiconductor nanorods and transfer-printed micro-silicon solar cells," ACS Nano **8**, 44–53 (2014).
16. I. Sychugov, "Analytical description of a luminescent solar concentrator," Optica **6**, 1046–1049 (2019).
17. R. Soti, E. Farkas, M. Hilbert, Z. Farkas, and I. Ketskemety, "Photon transport in luminescent solar concentrators," J. Lumin. **68**, 105–114 (1996).

18. M. S. Decardona, M. Carrascosa, F. Meseguer, F. Cusso, and F. Jaque, "Edge effect on luminescent solar concentrators," Solar Cells **15**, 225–230 (1985).
19. A. Marinins, R. Shafagh, W. Van der Wijngaart, T. Haraldsson, J. Linnros, J. G. C. Veinot, S. Popov, and I. Sychugov, "Light converting polymer/Si nanocrystal composites with stable 60–70% efficiency and their glass laminates," ACS Appl. Mater. Interfaces **9**, 30267–30272 (2017).
20. S. K. E. Hill, R. Connell, C. Peterson, J. Hollinger, M. A. Hillmyer, U. Kortshagen, and V. E. Ferry, "Silicon quantum dot–poly(methylmethacrylate) nanocomposites with reduced light scattering for luminescent solar concentrators," ACS Photon. **6**, 170–180 (2019).
21. J. Huang, J. Zhou, A. Clemments, H. Sugimoto, M. Fujii, T. Haraldsson, B. Xu, and I. Sychugov, Triplex glass laminates with Si quantum dots for luminescent solar concentrators, arXiv:2003.12131 (2020).
22. I. Sychugov, Origin file with formulas for a square (2019): https://doi.org/10.6084/m9.figshare.12338384
23. I. Sychugov ,Origin file with formulas for a rectangle (2019): https://doi.org/10.6084/m9.figshare.12338387